ACS Photonics

Article

pubs.acs.org/journal/apchd5

Near Infrared to Visible Electroluminescent Diodes Based on Organometallic Halide Perovskites: Structural and Optical Investigation

Naresh K. Kumawat,[†] Amrita Dey,[†] K. L. Narasimhan,[‡] and Dinesh Kabra*[,†]

Departments of [†]Physics and [‡]Electrical Engineering, Indian Institute of Technology Bombay, Powai, Mumbai India, 400076

Supporting Information

ABSTRACT: In this paper we present a study of the structural, electrical, and optical properties of four different 3D organometallic halide-based perovskite semiconductors with band gaps varying from NIR to visible at room temperature. Electroluminescent devices (using a solution process) with these perovskites as the active layer are also demonstrated. The morphology and crystallinity of the perovskite depends on the halide ion and substrate wetting conditions, where crystallite size varies from ~100s nm to few micrometers. We found it has a huge influence on the optical properties and performance of light emitting diodes (LEDs) using these perovskites as the active layer. Photoluminescence studies in the presence of commonly used charge injection layers are also studied and we correlate these results with performance of PeLEDs. We also demonstrate additional control of the electroluminescence emission by the formation of new complexes with organic hole transport layers. Finally, we clarify the diverse electronic charge transport in these perovskites. These results show promise of a new materials regime for LEDs.

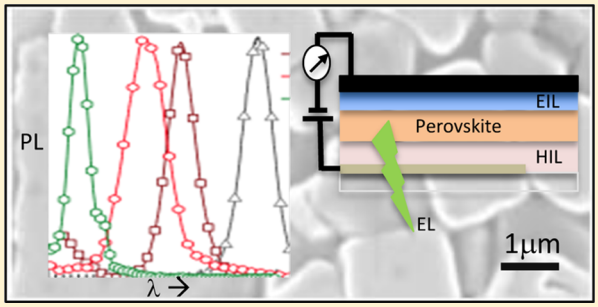

KEYWORDS: *perovskites, structure and morphology, PL efficiency, charge injection/transport, LEDs*

There is a great interest in the development of solid-state light-emitting devices due to their continuously increasing demand coupled with the disadvantages of fluorescence tube-light and incandescent bulb-light.[1] Efficient light generation has been realized in inorganic semiconductors with direct band gaps, such as GaAs and GaN, but these are costly and difficult to process hence not much used in large-area displays. Polycrystalline ZnS-based systems have been developed for large area displays by Destriau in 1936,[2] however, low efficiencies and poor reliability have prevented large-scale production. Recently, organometal halides ($CH_3NH_3PbX_3$ = ABX_3, where A = $CH_3NH_3^+$, B = divalent metal, that is, Pb^{2+} and X^- = halide ion) based perovskite semiconductors have shown excellent performance in solar cells[3−6] application and optical gain studies by NTU, Cambridge and Sargent's group[7−9] and therefore raise a great possibility of efficient light emission by these direct band gap crystalline semiconductors through charge carrier injection under an applied field (electroluminescence, i.e., EL).[10] These systems have the advantage that the band gap can be easily tuned by substitution of R-NH_3 group, metal or halide. Light-emitting devices based on perovskites have been reported in the past;[11−13] however, EL could only be achieved at low temperature (77 K), which made it unrealistic for lighting/display application. There is a nice effort from Mitzi's group to get EL at room temperature in layered perovskites by introducing dye cation, hence emission in those devices were coming from purely organic component.[14] Here, we report NIR to visible EL diodes based on organometallic halide perovskites (PeLEDs) at room temperature with biasing voltages below 5 V. Tan et al. and Lee et al. have recently shown an excellent operation of such PeLEDs.[10,15] Band gap of semiconductor is varied by either changing of halide ion or by using mixed halide ion compositions.[16] This paper relates structural, morphological, optical, and electrical properties of these novel materials. Sample preparation, device fabrication, and experimental processes are available in Supporting Information.

RESULTS AND DISCUSSION

Structural and Morphological Studies. In this section we report on the structural and morphology studies of the deposited thin films of different band gaps perovskite semiconductors. The perovskites typically crystalline in a cubic or tetragonal structure depending on the concentration of Cl and Br.[17,18] Figure 1a shows the tetragonal crystal structure with respective positions of $CH_3NH_3^+$, Pb^{2+}, and X^- ions. Figure 1c shows the X-ray diffraction (XRD) pattern for NIR emissive ($ABI_{3-x}Cl_x$), red emissive ($ABI_{1.19}Br_{1.37}Cl_{0.44}$, and $ABI_{1.25}Br_{1.75}$), and green emissive ($ABBr_3$) thin film after annealing. The diffraction peak occurs at ~14° for iodine cation and progressively moves to higher angles as the cation size decreases (Figure 1c and Table 1). The interplanar distance (d)

Received: October 7, 2014
Published: January 27, 2015

DOI: 10.1021/acsphotonics.5b00018
ACS Photonics 2015, 2, 349−354

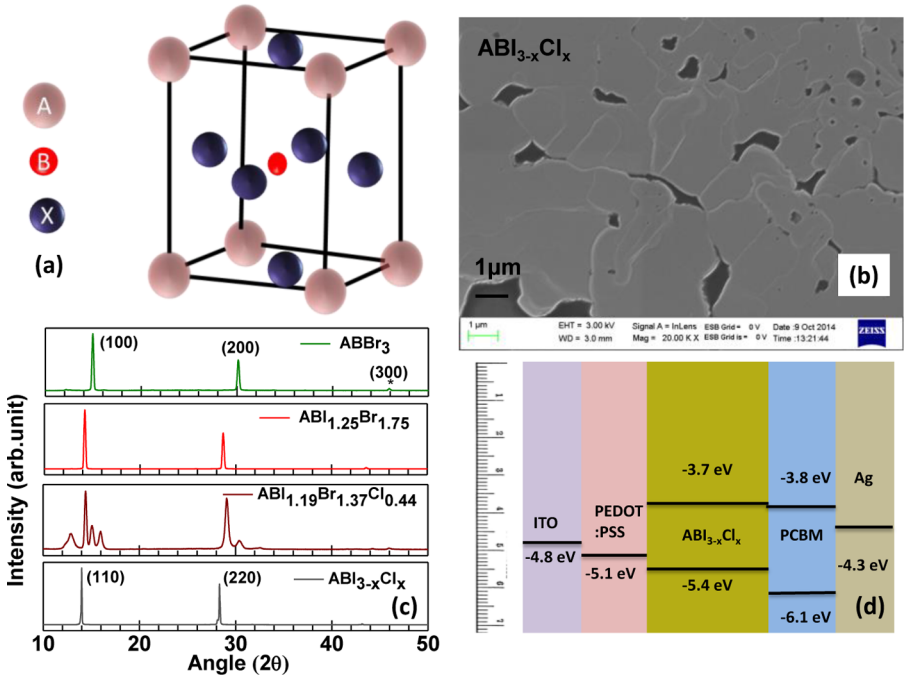

Figure 1. Structural and morphological studies: (a) Typical crystal structure of organometallic halide (ABX_3) where A is for alkylamine ($R\text{-}NH_3$), B is for divalent metal (Pb^{2+}), and X is for halide ion (X^-). (b) FESEM image of $ABI_{3-x}Cl_x$ perovskite film on PEDOT:PSS-coated glass substrate. (c) XRD pattern for annealed film of four perovskites materials with a change of halide component in ABX_3 configuration on glass substrate. (d) Electroluminescent diodes structure based on $ABI_{3-x}Cl_x$, energy level values are taken from literature.[22]

Table 1. XRD Studies To Determine Interplanar Spacing (d) and fwhm of First Order Diffraction Peak of Various Annealed Perovskites Film Prepared on Glass Substrates

perovskite	2θ (°)	experimental interplanar distance (d) in Å	fwhm corresponding to first order peak (°)
$ABBr_3$	14.9	5.9	0.21
$ABI_{1.25}Br_{1.75}$	14.2	5.8	0.18
$ABI_{1.19}Br_{1.37}Cl_{0.44}$	14.4	6.1	0.20
$ABI_{3-x}Cl_x$	14	6.3	0.07

is determined by the 2θ peak positions using Bragg's law ($n\lambda = 2d \sin\theta$).[19] These results are in agreement with the values of diffraction angle peak for tetragonal phase for $ABI_{3-x}Cl_x$5[20] and cubic phase for $ABI_{1.25}Br_{1.75}$ and $ABBr_3$ (Figure S2 and Table S1).[16,17] There is a slight shift of 2θ peak positions in the case of $ABI_{3-x}Cl_x$ and $ABI_{1.25}Br_{1.75}$ perovskite film's diffraction results from pure ABI_3 peak after annealing (see in Figure S2). Shift of 2θ peak is expected to happen by mixing of Br and Cl along with I in these perovskite structures. However, $ABI_{1.19}Br_{1.37}Cl_{0.44}$ is the mixed phase of all the three perovskites with slightly broader diffraction peak implying smaller crystalline domains as observed FESEM image. An extra peak at $2\theta \sim 12°$ corresponds to $PbX_{2.5}$. We now discuss the morphology of these films.

Figures S4 and S5 show the morphology of the different perovskite films deposited on glass and PEDOT:PSS-coated substrates. The coverage is poor for all the films deposited on glass. Significantly improved coverage is seen for films deposited on PEDOT:PSS-coated substrates, as it is seen in Figure 1b for the morphology of $ABI_{3-x}Cl_x$ (reproduced again in Figure S5c). We obtained on the average big crystallite domain size (few micrometers long) for $ABI_{3-x}Cl_x$. The $ABBr_3$ film shows brick-like crystalline domains with size varying from submicrometer to 5 μm (Figure S4a). The morphology of $ABI_{1.19}Br_{1.37}Cl_{0.44}$ films are shown in Figure S5a,b. Crystallite size for $ABI_{1.25}Br_{1.75}$ are of intermediate size and $ABI_{1.19}Br_{1.37}Cl_{0.44}$ films have smallest domains with clear observations of distinct $ABBr_3$ crystallite domain's presence in these films. Variation in average grain size for different perovskite is expected to influence the electronic properties of these semiconductor films.[21] Stoichiometry analysis is also carried out for all these films using energy dispersive X-ray analysis (EDX) mode of FESEM and respective quasi-halide components are mentioned as subscript for these in respective FESEM images (Figures S4 and S5). In the case of $ABI_{3-x}Cl_x$, Cl is below detection limits.

Figure 1d shows the typical device structure used for most of EL diodes. The energy level values are taken from literature.[22] Energy levels for three other perovskites semiconductors with respect to charge injection layers are shown in Supporting Information in Figure S1.

Optical Studies. We have also carried out optical studies on these perovskite films with various band gaps covering the Vis-NIR electromagnetic spectrum. Figure 2a shows UV−vis absorption spectra with respect to incident light energy for $ABBr_3$, $ABI_{1.25}Br_{1.75}$, $ABI_{1.19}Br_{1.37}Cl_{0.44}$, and $ABI_{3-x}Cl_x$ films after annealing. As expected with increasing iodine content, the band gap red shifts from 2.3 to 1.6 eV, as shown in Table 2 (see Figure S6). Band gap for these perovskite semiconductors are measured using the relation $\alpha h\nu = A(h\nu - E_g)^{1/2}$.[23] The band edge of $ABI_{3-x}Cl_x$ and $ABBr_3$ films are steeper than that of $ABI_{1.25}Br_{1.75}$ and $ABI_{1.19}Br_{1.37}Cl_{0.44}$ perovskites. The Urbach energy is determined by the slope of log{absorption coefficient} versus energy spectra below the bandgap (see Table 2 and Figure S7) and is a measure of the disorder in the semiconductor.[24] From the values of the Urbach energy (Table 2), we conclude that the disorder is larger in $ABI_{1.25}Br_{1.75}$ and

DOI: 10.1021/acsphotonics.5b00018
ACS Photonics 2015, 2, 349−354

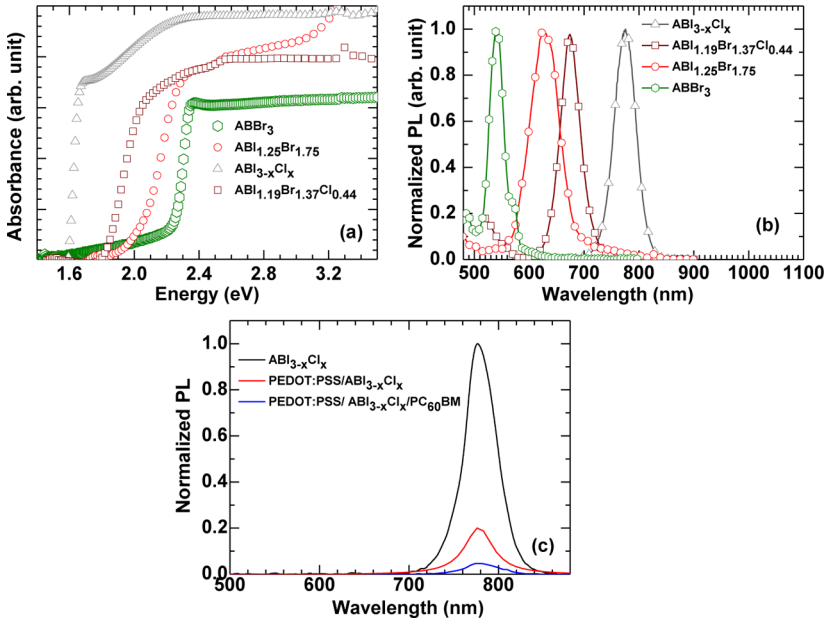

Figure 2. Optical properties of perovskites. (a) UV−vis absorbance spectra on energy scale for all four perovskite. (b) Photoluminescence spectra of perovskite semiconductor film prepared on quartz substrates with excitation wavelength corresponds to their UV−vis spectra. (c) Quenching of PL at different interlayer for $ABI_{3-x}Cl_x$ on quartz substrates with excitation wavelength of 650 nm.

Table 2. UV-Vis Band-Gap and Respective Urbach Energy for Perovskite Semiconductor Films

perovskite	band gap (in eV)	Urbach energy (E_u; in meV)
$ABBr_3$	2.31	41
$ABI_{1.25}Br_{1.75}$	2.15	125
$ABI_{1.19}Br_{1.37}Cl_{0.44}$	1.93	126
$ABI_{3-x}Cl_x$	1.6	59

$ABI_{1.19}Br_{1.37}Cl_{0.44}$ films. This can be attributed to mixed smaller domains as seen in the case of XRD studies in Figure 1b and in FESEM images (see in Figures S4 and S5). Absorption beyond the Urbach tail can be attributed to deeper defect states in these films.[25,17]

Figure 2b shows the photoluminescence (PL) spectra of all four perovskite films. Peak wavelength and respective width of the PL emission peak is shown in Table 3. As expected, the PL peak position moves to longer wavelengths (green to NIR) with increasing substitution of Br with Iodine.

Table 3. PL and EL Emission Peak and Corresponding fwhm

perovskite	$\lambda_{PL,peak}$ (nm)	PL fwhm (nm)	$\lambda_{EL,peak}$ (nm)	EL fwhm (nm)
$ABBr_3$	541	30.60	515	30.90
$ABI_{1.25}Br_{1.75}$	627	62.60	707	90.30
$ABI_{1.19}Br_{1.37}Cl_{0.44}$	674	43.40	760	40.60
$ABI_{3-x}Cl_x$	774	45.90	771	32.70

In order to fabricate PeLEDs, we shall need to introduce charge injection/transport layers adjacent to these semiconductor films. Hence, we studied the effect on PL due to the presence of charge injection/transport layers.

PL quenching of $ABI_{3-x}Cl_x$ is observed due to adjacent charge transporting layers (PEDOT:PSS/$ABI_{3-x}Cl_x$ and $ABI_{3-x}Cl_x$/$PC_{60}BM$), as shown in Figure 2c. We observed PL quenching due to both PEDOT:PSS and $PC_{60}BM$ in ∼320 nm thick $ABI_{3-x}Cl_x$ film on optical excitation. It can be attributed to long diffusion length of charge carriers in $ABI_{3-x}Cl_x$.[26] We did this for other three perovskite films as well for which PL spectra are shown in Figure S8. PL intensity found to be higher in the case of $ABBr_3$ on PEDOT:PSS-coated substrate as compare to $ABBr_3$ film prepared on glass substrate, which can be attributed to poor coverage of $ABBr_3$ film on glass as compared to PEDOT:PSS-coated substrate. We also carried out absolute PL yield measurement of these films, in both neat films and films in proximity with the charge transporting layers. This was done by placing the perovskite film (smaller than detector area) directly on top of a calibrated large area photodetector and measuring the luminescence in AC mode.[27] In these measurements, only forward emission photons are measured. Scattered and wave-guided as substrate modes are not accounted for in the estimate of PL yield. The numbers in Table 4, hence, represent a lower bound to the quantum efficiency.

NIR PeLEDs. After structural and optical characterization of perovskites films, we fabricated PeLEDs with a device structure,

Table 4. Photoluminescence Quantum Efficiency (η_{PL}) of Various Perovskite Semiconductor Films with and without Charge Injection Interlayers

perovskite	interfaces	η_{PL}, forward (%)
ABI_xCl_{3-x}	glass/$ABI_{3-x}Cl_x$	17.6
	PEDOT:PSS/$ABI_{3-x}Cl_x$	9.5
	PEDOT:PSS/$ABI_{3-x}Cl_x$/$PC_{60}BM$	7.7
$ABBr_3$	glass/$ABBr_3$	3.7
	PEDOT:PSS/$ABBr_3$	6.3
	PEDOT:PSS/$ABBr_3$/$PC_{60}BM$	3.9
	PEDOT:PSS/TPD/$ABBr_3$/$PC_{60}BM$	2.9
$ABI_{1.19}Br_{1.37}Cl_{0.44}$	glass/$ABI_{1.19}Br_{1.37}Cl_{0.44}$	7.1
	PEDOT:PSS/$ABI_{1.19}Br_{1.37}Cl_{0.44}$	5.4
	PEDOT:PSS/TPD/$ABI_{1.19}Br_{1.37}Cl_{0.44}$	2
$ABI_{1.25}Br_{1.75}$	glass/$ABI_{1.25}Br_{1.75}$	4

DOI: 10.1021/acsphotonics.5b00018
ACS Photonics 2015, 2, 349−354

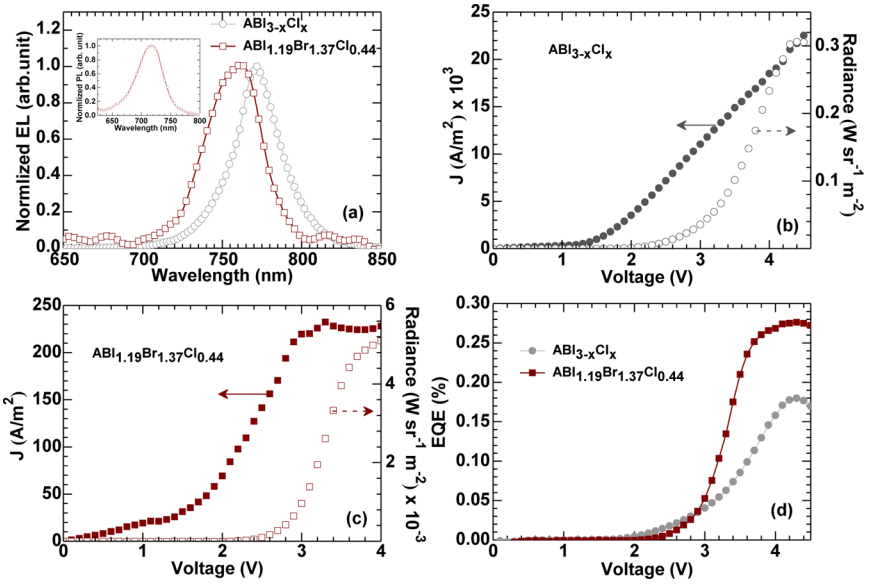

Figure 3. NIR electroluminescent diodes. (a) EL spectra from PeLEDs using $ABI_{3-x}Cl_x$ (circle) and $ABI_{1.19}Br_{1.37}Cl_{0.44}$ (square) perovskite semiconductor, inset shows the PL spectra from blend of TPD/$ABI_{1.19}Br_{1.37}Cl_{0.44}$ film with a ratio of 1:1, respectively. J-V-L characteristics of (b) ITO/PEDOT:PSS/$ABI_{3-x}Cl_x$/$PC_{60}BM$/Ag and (c) ITO/PEDOT:PSS/TPD/$ABI_{1.19}Br_{1.37}Cl_{0.44}$/Ag based PeLEDs. (d) EQE vs biasing voltage for NIR emissive PeLEDs derived from J-V-L curve and EL spectra.

as shown in Figure 1d. We fabricated PeLEDs using a device structure of ITO/PEDOT:PSS/$ABI_{3-x}Cl_x$ (or $ABI_{1.19}Br_{1.37}Cl_{0.44}$)/(with and without $PC_{60}BM$)/Ag. EL spectra of NIR emissive PeLEDs are shown in Figure 3a with their emission peak position and corresponding fwhm are shown in Table 3. $ABI_{3-x}Cl_x$ perovskite-based LED shows EL spectra in agreement with PL spectra, see Figure 2b and Figure 3a (Table 3). However, EL spectra of $ABI_{1.19}Br_{1.37}Cl_{0.44}$ mixed perovskite is found to be red-shifted by ~80 nm, that is, $\lambda_{PL,peak} \approx 674$ nm, whereas $\lambda_{EL,peak} \approx 760$ nm. We shall provide insight of this discrepancy in detail while discussing EL spectra of $ABI_{1.25}Br_{1.75}$ based PeLEDs in the next section of this paper. J-V-L characteristics of NIR emissive PeLEDs are shown in Figure 3b,c. Both of these diodes showed reasonable good diode characteristics with their knee voltages in the range of ~1.2 V. Table 5 summarizes the current density at 4 V bias and EQE for various PeLEDs. Current density numbers for these two diodes are found to be significantly different. Kahn et al. have shown that on alloying ABI_3 with Br (Cl), the conduction band level remains fixed and the valence band level gets deeper with increasing Br (Cl) content.[22] This implies that as the band gap increases, the hole injection barrier increases suitably. We hence expect a lower hole injection efficiency for $ABI_{1.19}Br_{1.37}Cl_{0.44}$ with respect to $ABI_{3-x}Cl_x$. In addition, $ABI_{3-x}Cl_x$ is less disordered than $ABI_{1.19}Br_{1.37}Cl_{0.44}$ as evidenced from the structural, morphological, and optical studies reported earlier. This qualitatively accounts for the difference in current density between the two samples.

Table 5. PeLEDs Parameters Extracted from Their J-V-L Characteristics

PeLED structure	@ 4 V J(A/m^2)	max. EQE (%) obtained
ITO/PEDOT:PSS/$ABI_{3-x}Cl_x$/$PC_{60}BM$/Ag	18500	0.18
ITO/PEDOT:PSS/TPD/$ABBr_3$/$PC_{60}BM$/Ag	5900	0.0013
ITO/PEDOT:PSS/TPD/$ABBr_3$/Ag	780	0.0065
ITO/PEDOT:PSS/TPD/$ABI_{1.25}Br_{1.75}$/$PC_{60}BM$/Ag	2700	0.0007
ITO/PEDOT:PSS/TPD/$ABI_{1.25}Br_{1.75}$/Ag	750	0.0011
ITO/PEDOT:PSS/TPD/$ABI_{1.19}Br_{1.37}Cl_{0.44}$/$PC_{60}BM$/Ag	10963	0.0073
ITO/PEDOT:PSS/TPD/$ABI_{1.19}Br_{1.37}Cl_{0.44}$/Ag	230	0.28
ITO/PEDOT:PSS/ABBr3/F8/Ca/Ag	4380	0.00002

In Figure 3c, typical J-V-L characteristics are shown for $ABI_{1.19}Br_{1.37}Cl_{0.44}$ based PeLEDs without $PC_{60}BM$ layer. The J-V-L characteristics of devices with $PC_{60}BM$ layer also are shown in Figure S9 and device structures with energy levels are shown in Figure S1c. These results are reproducible as four different batches of devices are prepared and in each batch there were 16 PeLEDs, with a sampling size of 64. The lower EL efficiency observed in the case of devices with $PC_{60}BM$ can be explained from PL quenching studies shown earlier (Tables 4 and 5). Hence, we emphasize here that with proper band alignment and passivation layers to prevent quenching, much more efficient device operation is possible.[15]

Figure 3d shows EQE versus applied bias, which shows better performance for $ABI_{1.19}Br_{1.37}Cl_{0.44}$ PeLED, which can be due to reduced quenching, as this PeLED structure did not have $PC_{60}BM$ layer. However, we note that, for $ABI_{1.19}Br_{1.37}Cl_{0.44}$ based PeLED (a Br containing perovskite), this is so far the highest EQE (0.28%) in literature for this device structure, and $ABI_{3-x}Cl_x$ also shows good EQE with a scope to improve each of these PeLEDs by proper charge injecting contact which do not quench EL.

Red and Green PeLEDs. Visible PeLEDs are also fabricated with ITO/PEDOT:PSS/TPD/$ABBr_3$ (or $ABI_{1.25}Br_{1.75}$)/($PC_{60}BM$ or without $PC_{60}BM$)/Ag device structures (TPD is *N*,*N*′-bis(3-methylphenyl)-*N*,*N*′-diphenyl-benzidine).[28] Figure 4a shows EL spectrum of PeLEDs in green and red color of EM spectrum with EL peak at 515 and 707 nm, respectively. EL emission peak is red-shifted by 80 nm with respect to PL peak for $ABI_{1.25}Br_{1.75}$ and $ABI_{1.19}Br_{1.37}Cl_{0.44}$ (Figure 3a) based PeLEDs. However, devices with and without

DOI: 10.1021/acsphotonics.5b00018
ACS Photonics 2015, 2, 349−354

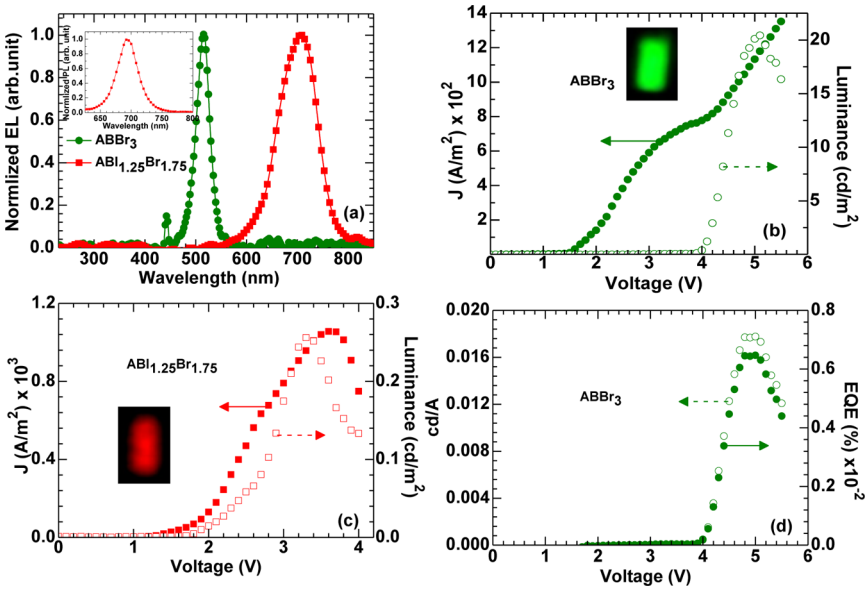

Figure 4. Visible electroluminescent diodes (a) EL spectra from PeLEDs using $ABBr_3$ (circle) and $ABI_{1.25}Br_{1.75}$ (square) perovskite semiconductors, inset shows PL from the blend of TPD:$ABI_{1.25}Br_{1.75}$ film with a ratio of 1:1, respectively. J-V-L characteristics of (b) ITO/PEDOT:PSS/TPD/$ABBr_3$/Ag (green) and (c) ITO/PEDOT:PSS/TPD/$ABI_{1.25}Br_{1.75}$/Ag (red) based PeLEDs with insets of operational PeLED picture. (d) EQE vs biasing voltage and luminance efficiency (cd/A) vs biasing voltage for green PeLEDs derived from J-V-L curve and EL spectra.

$PC_{60}BM$ interlayer showed similar EL spectra. We hence anticipate that the red shift might be due to a TPD perovskite complex at interface. To verify this hypothesis, we studied the PL of TPD/perovskite blends.

The inset in Figures 3a and 4a shows the PL of a TPD:perovskite blend in a 1:1 ratio. In the case of $ABI_{1.25}Br_{1.75}$ based PeLEDs we found PL of blend film (perovskite:TPD) and EL spectrum matched. The EL for this system is hence primarily due to a perovskite-TPD complex. In the case of $ABI_{1.19}Br_{1.37}Cl_{0.44}$ based PeLEDs the EL peak (760 nm) was slightly more red-shifted than PL peak (720 nm) from blend film. EL in this case can be due to CT-emission at TPD:perovskite interface. These results suggest that the EL in these devices takes place close to the anode. This implies electron mobility is much larger than the hole mobility in these device. This is consistent with the fact that no EL is seen close to the PL peak emission. Whereas, we note that there is a blue shift of ∼25 nm (corresponding energy difference is ∼100 meV) with respect to PL in EL of $ABBr_3$ based PeLEDs (see in Figures 2b and 4a and Table 3). Origin of this blue shift is not clear at this stage; however, it might be related to free carrier emission peak.[29,7]

Figure 4b,c shows J-V-L characteristics of visible color emitting PeLEDs in device structure of ITO/PEDOT:PSS/TPD/$ABBr_3$ or $ABI_{1.25}Br_{1.75}$/Ag, respective energy level diagram for these structures are shown in Figure S1a,b. Figure 4d shows the EQE vs bias voltage and luminance efficiency (cd/A) versus voltage for green PeLEDs, which are in agreement with Figure 4a,b.

We see from Table 5 that diodes without a $PC_{60}BM$ (EIL layer) layer show significantly smaller current density. While $PC_{60}BM$ facilitates electron injection, the EL efficiency is reduced in these devices due to quenching (Table 4). From the PL yield analysis (Table 4), one would have expected the EQE to be smaller by a factor of 2 for a device with $PC_{60}BM$ as EIL. However, the EQE drops by about a factor of 5 (with $PC_{60}BM$ as EIL, Table 5). This suggests that the absence of the $PC_{60}BM$ layer facilitates charge carrier balance.

Inset of Figure 4b,c shows the picture of operational PeLEDs taken by normal camera. We confirm that $ABBr_3$ with this similar device structure is has at least two orders higher EQE than earlier reports in similar device structures and luminance value is also high by more than one order. As most of these PeLEDs are made without $PC_{60}BM$ interlayer and we found improvement in EQE with a price of higher operating voltages. Lee et al., however, have recently shown great improvement in $ABBr_3$-based PeLEDs by introducing an interlayer to improve charge carrier balance and prevent EL quenching.[15]

CONCLUSION

In conclusion, we have studied the influence of structural, morphological, and optical properties on LED performance for four different band gap 3D perovskite semiconductors. Both morphology and grain size is influenced by the choice of the halide ion composition. This, in turn, is related to disorder, which influences electrical and optical properties of the perovskite.

It is important to note that good wetting of the contact by the perovskite layer is very important for obtaining low leakage devices. Our studies show that PEDOT:PSS and TPD as contact layers facilitate wetting of the perovskite layer. We also show that interdiffusion of TPD in perovskites forms a new complex which results in significantly red-shifted EL. This allows an additional parameter for device design. However, we show that these layers also quench the luminescence reducing the efficiency of the EL devices. We would like to point out that the use of $PC_{60}BM$ and PEDOT:PSS as electron and hole transport layers, respectively, results in a significantly reduced EL intensity due to quenching. This study points to the need of looking at other transport layers, which can result in significantly improved EL efficiency without compromising the morphology of the grown films. These PeLEDs have a

DOI: 10.1021/acsphotonics.5b00018
ACS Photonics 2015, 2, 349−354

potential of future electrical injection laser diodes and lighting applications.

■ ASSOCIATED CONTENT

Supporting Information

Material synthesis and methods, Figures S1−S13, Table S1, and relevant references. This material is available free of charge via the Internet at http://pubs.acs.org.

■ AUTHOR INFORMATION

Notes

The authors declare no competing financial interest.

■ ACKNOWLEDGMENTS

This work is partially supported by the IITB Seed Grant (12IRCCSG044). We also acknowledge support of Center of Excellence in Nanoelectronics (CEN) for device fabrication facility and National Center for Photovoltaic Research and Education (NCPRE) for characterization of morphology. Authors acknowledge Prof. Anil Kumar from Chem. IITB-Mumbai for providing synthesis facility. A.D. acknowledges UGC for research fellowship.

■ REFERENCES

(1) Humphreys, C. J. Solid-State Lighting. *MRS Bull.* **2008**, *33*, 459.
(2) Destriau, G. AC Electroluminescence in ZnS. *J. Chem. Phys.* **1936**, *33*, 589.
(3) (i) Lee, M. M.; Teuscher, J.; Miyasaka, T.; Murakami, T. N.; Snaith, H. J. Efficient Hybrid Solar Cells Based on Meso-Superstructured Organometal Halide Perovskites. *Science* **2012**, *338*, 643−647. (ii) Liu, M.; Johnston, M. B.; Snaith, H. J. Efficient Planar Heterojunction Perovskite Solar Cells by Vapour Deposition. *Nature* **2013**, *501*, 395−398.
(4) Burschka, J.; pellet, N.; Moon, S.-J.; Humphry-Baker, R.; Gao, P.; Nazeeruddin, M. K.; Gratzel, M. Sequential Deposition as a Route to High-Performance Perovskite-Sensitized Solar Cells. *Nature* **2013**, *499*, 316−319.
(5) Zhou, H.; Chen, Q.; Li, G.; Luo, S.; Song, T.-B.; Duan, H.-S.; Hong, Z.; You, J.; Liu, Y.; Yang, Y. Interface Engineering of Highly Efficient Perovskite Solar Cells. *Science* **2014**, *345*, 542.
(6) Edri, E.; Kirmayer, S.; Mukhopadhyay, S.; Gartsman, K.; Hodes, G.; Cahen, D. Elucidating the Charge Carrier Separation and Working Mechanism of $CH_3NH_3PbI_{3-x}Cl_x$ Perovskite Solar Cells. *Nat. Commun.* **2014**, *5*, 3461−3469.
(7) Xing, G.; Mathews, N.; Sien Lim, S.; Yantara, N.; Liu, X.; Sabba, D.; Grazel, M.; Mhaisalkar, S.; Sum, T. C. Low-Temperature Solution-Processed Wavelength-Tunable Perovskites for Lasing. *Nat. Mater.* **2014**, *13*, 476−480.
(8) Deschler, F.; Price, M.; Pathak, S.; Klintberg, L. E.; Jarausch, D.-D.; Higler, R.; Huttner, S.; Leijtens, T.; Stranks, S. D.; Snaith, H. J.; Atature, M.; Phillips, R. T.; Friend, R. H. High Photoluminescence Efficiency and Optically Pumped Lasing in Solution-Processed Mixed Halide Perovskite Semiconductors. *J. Phys. Chem. Lett.* **2014**, *5*, 1421−1426.
(9) Sutherland, B. R.; Hoogland, S.; Adachi, M. M.; Kanjanaboos, P.; Wong, C. T. O.; McDowell, J. J.; Xu, J.; Voznyy, O.; Ning, Z.; Houtepen, A. J.; Sargent, E. H. Perovskite Thin Films via Atomic Layer Deposition. *Adv. Mater.* **2015**, *27*, 53−58.
(10) Tan, Z.-K.; Moghaddam, R. S.; Lai, M. L.; Docampo, P.; Higler, R.; Deschler, F.; Price, M.; Sadhanala, A.; Pazos, L. M.; Credgington, D.; Hanusch, F.; Bein, T.; Snaith, H. J.; Friend, R. H. Bright Light-Emitting Diodes Based on Organometal Halide Perovskite. *Nat. Nanotechnol.* **2014**, *9*, 687−692.
(11) Hattori, T.; Takahiro; Era, M.; Tsutsui, T.; Saito, S. Highly Efficient Electroluminescence from a Heterostructure Device Combined with Emissive Layered-Perovskite and an Electron-Transporting Organic Compound. *Chem. Phys. Lett.* **1996**, *254*, 103−108.
(12) Era, M.; Morimoto, S.; Tsutsui, T.; Saito, S. Organic-Inorganic Heterostructure Electroluminescent Device using a Layered Perovskite Semiconductor $(C_6H_5C_2H_4NH_3)_2PbI_4$. *Appl. Phys. Lett.* **1994**, *65*, 676.
(13) Schmidt, L.; Pertegas, A.; Gonzalez-Carrero, S.; Malinkiewicz, O.; Agouram, S.; Espallargas, G. M.; Bolink, H. J.; Galian, R. E.; Perez-Prieto, J. Nontemplate Synthesis of $CH_3NH_3PbBr_3$ Perovskite Nanoparticles. *J. Am. Chem. Soc.* **2014**, *136*, 850−853.
(14) Chondroudis, K.; Mitzi, D. B. Electroluminescence from an Organic-Inorganic Perovskite Incorporating a Quaterthiophene Dye within Lead Halide Perovskite Layers. *Chem. Mater.* **1999**, *11*, 3028−3030.
(15) Kim, Y. H.; Cho, H.; Heo, J. H.; Kim, T. S.; Myoung, N.; Lee, C. L.; Im, S. H.; Lee, T. W. Multicolored Organic/Inorganic Hybrid Perovskite Light-Emitting Diodes. *Adv. Mater.* **2014**, DOI: 10.1002/adma.201403751.
(16) Noh, J. H.; Im, S. H.; Heo, J. H.; Mandal, T. N.; Seok, S. I. Chemical Management for Colorful, Efficient, and Stable Inorganic-Organic Hybrid Nanostructured Solar Cells. *Nano Lett.* **2013**, *13*, 1764−1769.
(17) Sadhanala, A.; Deschler, F.; Thomas, T. H.; Dutton, S. E.; Goedel, K. C.; Hanusch, F. C.; Lai, M. L.; Steiner, U.; Bein, T.; Docampo, P.; Cahen, D.; Friend, R. H. Preparation of Single-Phase Films of $CH_3NH_3Pb(I_{1-x}Br_x)_3$ with Sharp Optical Band Edges. *J. Phys. Chem. Lett.* **2014**, *5*, 2501−2505.
(18) Aharon, S.; Cohen, B. E.; Etgar, L. Hybrid Lead Halide Iodide and Lead Halide Bromide in Efficient Hole Conductor Free Perovskite Solar Cell. *J. Phys. Chem. C* **2014**, *118* (30), 17160−17165.
(19) Cullity, B. D.; Stock, S. R. *Elements of X-ray Diffraction*, 3rd ed.; Prentice Hall: New Jersey, 2001.
(20) Kitazawa, N.; Watanabe, Y.; Nakamura, Y. Optical Properties of $CH_3NH_3PbX_3$ (X = Halogen) and Their Mixed-Halide Crystals. *J. Mater. Sci.* **2002**, *37*, 3585−3587.
(21) D'Innocenzo, V.; Kandada, A. R. S.; Bastiani, M. D.; Gandini, M.; Petrozza. Tuning the Light Emission Properties by Band Gap Engineering in Hybrid Lead Halide Perovskite. A. *J. Am. Chem. Soc.* **2014**, *136*, 17730.
(22) Schulz, P.; Edri, E.; Kirmayer, S.; Hodes, G.; Cahen, D.; Kahn, A. Interface Energetic in Organo-Metal Halide Perovskite-Based Photovoltaic Cells. *Energy Environ. Sci.* **2014**, *7*, 1377−1381.
(23) Yu, P. Y.; Cardona, M. *Fundamentals of Semiconductors (Physics and Materials Properties)*, 4th ed.; Springer: New York, 2010.
(24) Venkateshvaran, D.; Nikolka, M.; Sadhanala, A.; Lemaur, V.; Zelazny, M.; Kepa, M.; Hurhangee, M.; Kronemeijer, A. J.; Pecunia, V.; Nasrallah, J.; Romanov, I.; Broch, K.; McCulloch, I.; Emin, D.; Olivier, Y.; Cornil, J.; Beljonne, D.; Sirringhaus, H. Approaching Disorder-free Transport in High-Mobility Conjugated Polymers. *Nature* **2014**, *515*, 384−388.
(25) Urbach, F. The Long-Wavelength Edge of Photographic Sensitivity and of the Electronic Absorytion of Solids. *Phys. Rev.* **1953**, *92*, 1324−1333.
(26) Stranks, S. D.; Eperon, G. E.; Grancini, G.; Menelaou, C.; Alcocer, M. J. P.; Leijtens, T.; Herz, L. M.; Petrozza, A.; Snaith, H. J. Electron-Hole Diffusion Lengths Exceeding 1 Micrometer in an Organometal Trihalide Perovskite Absorber. *Science* **2013**, *342*, 341.
(27) Lee, X. Y.; Wu, C. Q.; Verma, A. K.; Ranganathan, R.; Yablonovitch, E. 25th Photovoltaic Specialists Conference, Washington, DC, May 13−17, 1996, IEEE: New York, 1996; pp 141−142.
(28) Roldán-Carmona, C.; Malinkiewicz, O.; Betancur, R.; Longo, G.; Momblona, C.; Jaramillo, F.; Camacho, L.; Bolink, H. J. High Efficiency Single-Junction Semitransparent Perovskite Solar Cells. *Energy Environ. Sci.* **2014**, *7*, 2968−2973.
(29) D'Innocenzo, V.; Grancini, G.; Alcocer, M. J. P.; Kandada, A. R. S.; Stranks, S. D.; Lee, M. M.; Lanzani, G.; Snaith, H. J.; Petrozza, A. Excitons versus Free Charges in Organo-Lead Tri-Halide Perovskites. *Nat. Commun.* **2014**, *5*, 3586−3592.

DOI: 10.1021/acsphotonics.5b00018
ACS Photonics 2015, 2, 349−354